Abyssal Ocean Warming and Salinification after Weddell Polynyas in the GFDL CM2G Coupled Climate Model

HANNAH ZANOWSKI

Program in Atmospheric and Oceanic Sciences, Princeton University, Princeton, New Jersey

ROBERT HALLBERG

NOAA/Geophysical Fluid Dynamics Laboratory, Princeton, New Jersey

JORGE L. SARMIENTO

Program in Atmospheric and Oceanic Sciences, Princeton University, Princeton, New Jersey

(Manuscript received 9 June 2015, in final form 10 August 2015)

ABSTRACT

The role of Weddell Sea polynyas in establishing deep-ocean properties is explored in the NOAA Geophysical Fluid Dynamics Laboratory's (GFDL) coupled climate model CM2G. Using statistical composite analysis of over 30 polynya events that occur in a 2000-yr-long preindustrial control run, the temperature, salinity, and water mass changes associated with the composite event are quantified. For the time period following the composite polynya cessation, termed the "recovery," warming between 0.002° and 0.019°C decade^{-1} occurs below 4200 m in the Southern Ocean basins. Temperature and salinity changes are strongest in the Southern Ocean and the South Atlantic near the polynya formation region. Comparison of the model results with abyssal temperature observations reveals that the 1970s Weddell Polynya recovery could account for 10% ± 8% of the recent warming in the abyssal Southern Ocean. For individual Southern Ocean basins, this percentage is as little as 6% ± 11% or as much as 34% ± 13%.

1. Introduction

In the mid-1970s, a large opening, later referred to as the Weddell Polynya, was observed in the Antarctic sea ice over the entirety of the 1974, 1975, and 1976 austral winters. With an area of 2–3 × 10^5 km^2 (Carsey 1980; Martinson et al. 1981), a vast quantity of relatively warm water in the Weddell Sea was mixed upward and exposed to the frigid Antarctic atmosphere. This caused an average oceanic heat loss of ~150 W m^{-2} (Moore et al. 2002; Gordon et al. 2007) over the three winters. Heat loss to the atmosphere assisted in the formation of dense water that sank to 3000 m (Comiso and Gordon 1987; Gordon 1991) in the Weddell Sea and initialized further convection through the upwelling of warmer deep waters. Given that the Weddell Sea is a primary location of Antarctic Bottom Water (AABW) formation (Seabrooke et al. 1971; Gill 1973; Carmack and Foster 1975a,b; Foster and Carmack 1976a,b; Orsi et al. 1999), it is possible that a polynya of this magnitude could impact the temperature and salinity structure in the global abyssal oceans. Observations indicate that the Weddell Polynya increased the rate of AABW formation in the Weddell Sea during the time it was actively convecting (Gordon 1982).

Modeling studies (e.g., Hirabara et al. 2012; Latif et al. 2013; Martin et al. 2013, 2015) further explore the possible impacts of the Weddell Polynya both within the ocean and in the climate system. These studies indicate that via intense heat loss to the atmosphere and changes to abyssal ocean temperature and salinity, a polynya of this magnitude has the potential to impact the climate system as a whole. Recent observations show deep and abyssal ocean warming (Robertson et al. 2002; Fahrbach

Denotes Open Access content.

Corresponding author address: Hannah Zanowski, Program in Atmospheric and Oceanic Sciences, Sayre Hall, 300 Forrestal Road, Princeton, NJ 08544.
E-mail: zanowski@princeton.edu

DOI: 10.1175/JPO-D-15-0109.1

et al. 2004; Johnson and Doney 2006; Johnson et al. 2007; Zenk and Morozov 2007; Meredith et al. 2008; Johnson et al. 2008; Fahrbach et al. 2011; Purkey and Johnson 2010, 2013), and Latif et al. (2013) were among the first to suggest that some of this warming was related to the Weddell Polynya through a rebound mechanism: an initial cooling from the polynya could lead to a warming many years after its cessation. This was likely the case in the Weddell Sea (Gordon 1982, 1991; Smedsrud 2005) and in the South Atlantic after the Weddell Polynya. Coles et al. (1996) attributed the late 1980s Argentine basin cooling to earlier Weddell Sea convection, and a decade later, Johnson and Doney (2006) provided observations of warming in the abyssal western South Atlantic basins. From 2005 to 2014, the abyssal Argentine basin and Scotia Sea warming were not detectable (Johnson et al. 2014). However, abyssal Brazil basin temperatures continued increasing over the same period, perhaps indicating northward propagation of the warming signal. These patterns of cooling followed by warming, as well as interbasin warming signal propagation, are consistent with a rebound from the Weddell Polynya.

The timing of the Weddell Polynya and its rebound in the deep ocean are coincident with anthropogenic climate change. Trends in deep-ocean temperature and salinity are likely to be indicators of climate change because dense water formation provides a direct link between the atmosphere and the abyssal oceans. In their observational studies, Purkey and Johnson (2010, 2012, 2013) conclude that both warming and freshening in the deep ocean, possibly attributable to anthropogenic climate change, contribute to sea level rise and increased heat storage as well as decreased AABW formation. Given that the rebound from the Weddell Polynya could also result in abyssal warming signals, we investigate the spatial and temporal variability of this transient phenomenon to determine the extent to which Weddell Sea convection affects abyssal ocean properties.

Despite recent emphasis on polynya-related abyssal ocean changes, previous modeling studies have two potentially serious issues: 1) they use Z-coordinate ocean models that are prone to spurious diapycnal mixing (Griffies et al. 2000; Ilicak et al. 2012), particularly in dense overflows and topographically constrained flows (Legg et al. 2006), and 2) only a small number of polynyas (<5) were used to draw conclusions about polynya-related changes in the abyssal oceans (e.g., Goosse and Fichefet 2001; Latif et al. 2013). Our study employs a coupled climate model with an isopycnal ocean component to investigate abyssal ocean temperature, salinity, and water mass changes associated with large polynyas in the Weddell Sea. We use composites consisting of over 30 polynyas that occur over a 2000-yr time period in the model to analyze these changes. We find that as much as 10% ± 8% of the observed warming in the abyssal Southern Ocean could be a result of the recovery after the Weddell Polynya.

2. Methods

a. Model

We use GFDL CM2G, a coupled land–atmosphere–ocean–sea ice model. CM2G is the physical component of GFDL's Earth System Model (ESM2G) (Dunne et al. 2012). It consists of the Generalized Ocean Layer Dynamics (GOLD) model (Adcroft and Hallberg 2006; Hallberg and Adcroft 2009); GFDL's Atmospheric Model, version 2 (AM2; Anderson et al. 2004); Land Model, version 3 (LM3.0; Milly et al. 2014); and the Sea Ice Simulator (SIS; Winton 2000). There is no biogeochemical component in CM2G, so surface chlorophyll is prescribed to account for its effect on radiation.

Our analysis is primarily concerned with abyssal ocean changes, so we chose to use a coupled model with an ocean component that best represents the dynamics and water mass structure in this region. Because GOLD is an isopycnal-coordinate model, it affords a natural space to represent density-driven currents and thus is particularly suited to simulate dense water overflows compared to Z-coordinate ocean models. Much of the deep water in the ocean is overflow water. Accurately representing these flows is necessary to correctly model deep-ocean water masses (Legg et al. 2006). In their study of Southern Ocean bottom water characteristics, Heuzé et al. (2013) found that ESM2G reasonably represents observed bottom water temperature, salinity, and density around Antarctica compared to 14 other CMIP5 models. We chose GOLD for this study because it is the ocean component of ESM2G and is therefore responsible for the formation of water with such properties.

GOLD is configured with 63 vertical layers. Four compose the bulk mixed layer—two for the mixed layer and another two that act as a buffer between the mixed layer and the isopycnal layers below. The remaining 59 layers compose the interior ocean and follow prescribed potential density values referenced to 2000 dbar. The horizontal spatial resolution is nominally 1° but refines to ⅓° in latitude near the equator. The full nonlinear equation of state is used for the dynamics.

b. Initialization

The model is initialized with 1860 preindustrial conditions and spun up for 3000 yr to achieve a quasi-steady state. An additional 2000 yr of the control simulation was run beyond the 3000-yr-long spinup, and our analysis focuses on these years. The extended spinup, coupled with

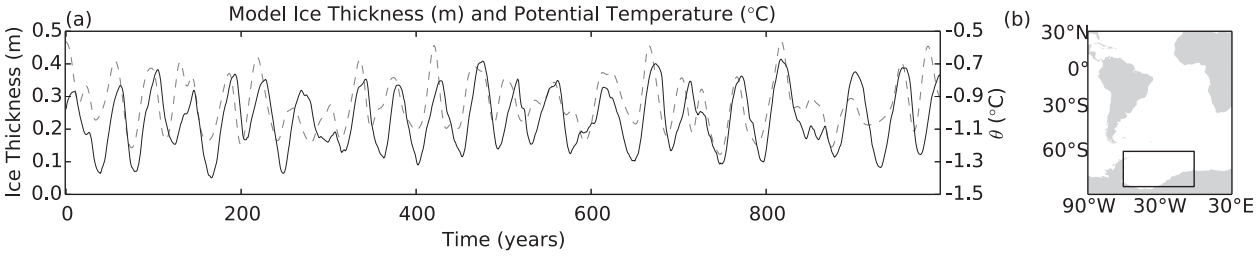

FIG. 1. (a) Time series of annually averaged sea ice thickness (dashed) and 1500–2500-m potential temperature (solid) (b) over 77°–60°S, 60°W–0° (box) in the Weddell Sea during the first 1000 yr of the simulation. To remove interannual variability, sea ice thickness has been low-pass filtered with a Butterworth filter (cutoff frequency of 0.1 yr^{-1}). Year 0 corresponds to the beginning of the time period after the model's 3000-yr spinup.

the low numerical mixing inherent to isopycnal ocean models (Ilicak et al. 2012), means that the model has very little drift ($\sim 5 \times 10^{-5}$ °C decade^{-1} for the Southern Hemisphere below 4200 m) in deep-ocean temperature.

c. *Polynya definition*

We use annually and volume-averaged Weddell Sea (77°–60°S, 60°W–0°; Fig. 1b) potential temperature between 1500 and 2500 m to detect polynyas. A total of 41 polynyas, represented as local temporal minima in the averaged temperature and sea ice thickness time series (Fig. 1a), occur during the 2000-yr-long simulation. Volume averaging over the deep Weddell Sea captures large subsurface temperature variations and simultaneously damps smaller-scale variability not directly attributable to polynyas. Annual averaging has a similar effect to volume averaging by removing seasonal variability, but it damps the polynya signals by including data from seasons when the Weddell Sea is not convecting. The polynya signals are still large enough to be distinguished in annually averaged output.

Our polynya definition differs from earlier literature (Carsey 1980; Comiso and Gordon 1987, 1996) that has often defined polynyas in terms of ice cover, as well as from recent literature such as de Lavergne et al. (2014), who used a mixed layer depth threshold to define Weddell Sea convection. The temperature metric is a more appropriate choice for this study. It accounts for some of the lag associated with the timing of sea ice minima in the Weddell Sea, which is when the polynyas occur, and the timing of deep-ocean changes, which occur years after the polynya. Weddell Sea potential temperature lags sea ice thickness (Fig. 1a) with a maximum correlation of 0.99 at a 14-yr lag, indicating that the temperature metric is capturing changes associated with polynyas in the Weddell Sea.

d. *Composites*

We take advantage of the regularity and large number of events in our simulation by using statistical composite analysis to determine the changes associated with a "typical" polynya. Compositing averages out spurious signals, making a more robust polynya signal than that achieved from analyzing only a small number of events.

We construct two types of composites to aid our analyses. The first composite (Fig. 2a) we refer to as the cooling composite. We define the zero year as the year when potential temperature in the Weddell Sea averaging region is decreasing most rapidly. This is often not the same year as when there is a corresponding local minimum in the sea ice (maximum rate of temperature decrease leads each sea ice minimum by 3 yr on average). However, it simulates the rapid deep-ocean temperature decrease that occurs during a polynya and appropriately represents the onset of convection.

We define the event length as the time in years between two successive temperature maxima in Fig. 1a. The event length varies from polynya to polynya, so it is useful to define two other quantities that we refer to as the preconvection onset time and postconvection recovery time. These average times are used to construct temporal bounds for the composite. Preconvection onset time is calculated by averaging the length of time between the year of the first temperature maximum in Fig. 2a and the zero year for all of the events. Similarly, postconvection recovery time is calculated by averaging the time between the zero year and the second temperature maximum in Fig. 2a for all of the events. The preconvection onset time for the cooling composite is 8 yr, and the postconvection recovery time is 41 yr, so we construct the cooling composite to begin 10 yr prior to the zero year and to end 45 yr after the zero year. The final event of the time series was truncated only 30 yr after the zero year, so it was excluded from the composite, leaving a total of 40 events.

As time after the zero year increases, individual polynya temperature signals begin to diverge (Fig. 2a), making the cooling composite less robust for those years. The recovery period analysis includes these later times. To achieve an upper bound for the recovery warming, we

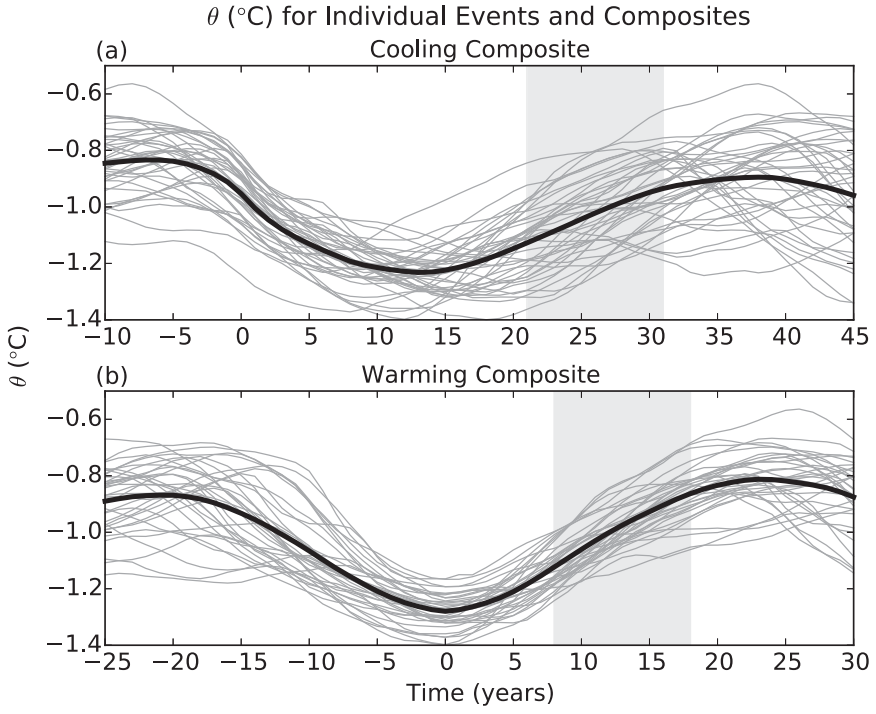

FIG. 2. Time series of annually and volume-averaged potential temperature in the Weddell Sea for (a) the cooling composite and (b) the warming composite (thick black lines). Single polynyas appear as thin gray lines. The volume average is taken over the region described in Fig. 1b. The gray shaded regions indicate the segment of the recovery period over which property changes were calculated for subsequent figures. In (a), year 0 corresponds to the time when temperature is decreasing the fastest. In (b), year 0 corresponds to the time when temperature reaches a minimum in the Weddell Sea. Six polynyas with the smallest post-zero-year warming trends (see text) are excluded from the warming composite.

construct a second composite (Fig. 2b) in which the zero year is shifted to the time when the deep Weddell Sea averaging region reaches its minimum temperature. We refer to this composite as the warming composite.

Several events in the warming composite had weak post-zero-year warming compared to the others. We determined post-zero-year warming trends for the events by fitting a line to each event's temperature data from years 5 to 20 (Fig. 2b) using linear least squares analysis. The weak recovery warming for these events is the result of secondary sea ice extent reductions in the Weddell Sea that occur after the zero year. It appears that the reduced sea ice extent again leads to subsurface cooling. For each weak event, this subsurface cooling is insufficient to create another temperature minimum in the Weddell Sea averaging region (Fig. 1) but instead acts to reduce the post-zero-year warming trend. Events composing the lowest 15% of the post-zero-year warming trends were excluded because they were nearly an order of magnitude lower than those of the remaining 85%. This left a total of 34 events in the warming composite.

e. *Deep property and water mass changes*

We define AABW as water denser than $\sigma_2 = 37.13\,\mathrm{kg\,m^{-3}}$ and use this definition to determine the annual-mean volume transport out of three regions of increasing size in the Weddell Sea and South Atlantic. Outward volume transport is calculated by vertically integrating water of density higher than $37.13\,\mathrm{kg\,m^{-3}}$ that is leaving each region. Anomalous volume transport is calculated by subtracting the long-term mean of the volume transport from the volume transport time series.

Basin-mean temperature changes below 4200 m are used to quantify the polynya recovery warming in the global abyssal oceans. A map of basin names and boundaries is provided (Fig. 3). We further partitioned four large Southern Hemisphere basins (Fig. 3) into regions based on the dynamics of the polynya signal and the large-scale deep circulation patterns (e.g., Wyrtki 1961; Reid 1989, 1997, 2003; Mantyla and Reid 1995). For example, we split the Weddell–Enderby basin into the Weddell basin and the Enderby basin and then further split the Enderby basin so that the northeastward flow around Conrad Rise

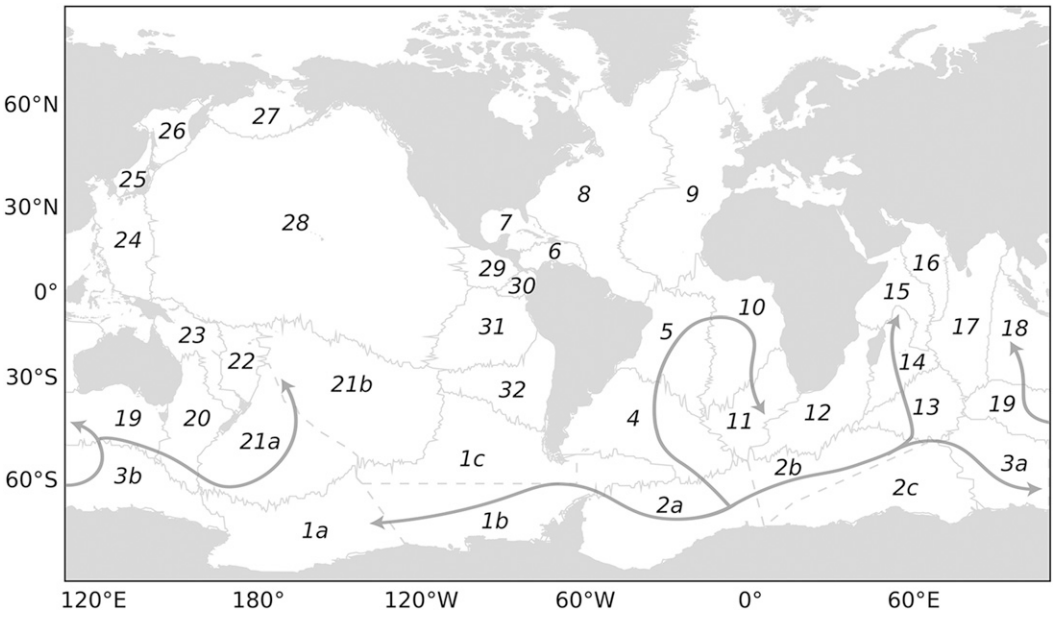

FIG. 3. Map of ocean basin boundaries with each of the 32 basins labeled. Solid basin boundaries are as in Purkey and Johnson (2010). In addition, dashed lines have been added to split four large southern basins. Thick gray lines indicate the spreading pathways of the polynya signal. Basin names are as follows: 1) Amundsen–Bellingshausen basin (ABB); 1a) Amundsen basin (AMB); 1b) southeast Pacific 1 (SE1); 1c) southeast Pacific 2 (SE2); 2) Weddell–Enderby basin (WEB); 2a) Weddell basin (WDB); 2b) Enderby 1 (EN1); 2c) Enderby 2 (EN2); 3) Australian–Antarctic basin (AAB); 3a) Australian–Antarctic 1 (AA1); 3b) Australian–Antarctic 2 (AA2); 4) Argentine basin (ARG); 5) Brazil basin (BRZ); 6) Caribbean basin (CRB); 7) Gulf of Mexico (GOM); 8) North Atlantic basin (NAB); 9) Iberian–Cape Canary basin (ICC); 10) Angola basin (ANG); 11) Cape basin (CPE); 12) Agulhas basin (AGH); 13) Crozet basin (CRZ); 14) Madagascar–Mascarene basin (MMB); 15) Somali basin (SMB); 16) Arabian basin (ARB); 17) mid-Indian basin (MIB); 18) Wharton basin (WHB); 19) South Australian basin (SAB); 20) Tasman basin (TSB); 21) southwest Pacific basin (SWP); 21a) southwest Pacific 1 (SW1); 21b) southwest Pacific 2 (SW2); 22) south Fiji basin (SFB); 23) Coral Sea basin (CSB); 24) Philippine basin (PHB); 25) Japan basin (JPB); 26) Kuril basin (KUB); 27) Aleutian–Bowers–Kamchatka basin (ABK); 28) North Pacific basin (NPB); 29) Guatemala basin (GAB); 30) Panama basin (PAB); 31) Peru–Bauer basin (PBB); and 32) Chile–Roggeveen basin (CHB).

(approximately 53°S, 41°E) would be separated from the westward return flow in the southern part of the basin. To quantify decadal warming rates in the abyssal basins, we take the mean of the annual temperature change over years 8 to 18 of the warming composite [Fig. 2b, gray box; analogous to years 21 to 31 of the cooling composite (Fig. 2a, gray box)] and multiply by 10 yr. Observed basin-mean warming rates are calculated by multiplying the Purkey and Johnson (2010) area-weighted depth averages of annual basin-mean warming rates below 4200 m by 10 yr. Following Purkey and Johnson (2010), areas for each basin at each depth are calculated from the satellite bathymetric dataset of Smith and Sandwell (1997).

3. Results

a. Composite sea ice and temperature

The temperature range over the event length is about 0.4°C for the cooling composite (Fig. 2a) and 0.5°C for the warming composite (Fig. 2b). Cooling composite (Fig. 2a) temperature decreases by about 0.3°C between the zero year and the time of minimum temperature (year 13), consistent with Gordon (1982), who reported maximum cooling of 0.4°C in the deep Weddell Sea after the Weddell Polynya. Robertson et al. (2002) reported Warm Deep Water (WDW) and Weddell Sea Deep Water (WSDW) cooling of a few tenths of a degree after the Weddell Polynya, as well as warming of about the same amount in subsequent decades. However, they found that the postpolynya warming in the deep Weddell Sea between 1500 and 2500 m was weak and not statistically significant.

Fractional sea ice extent annually averaged over the Weddell Sea (not shown) for both composites varies between 0.2 and 0.4 over the event length. Minimum and maximum fractional ice extent values for single polynyas range from 0.1 to 0.6. Composite sea ice extent maps yield no distinct region of minimum sea ice

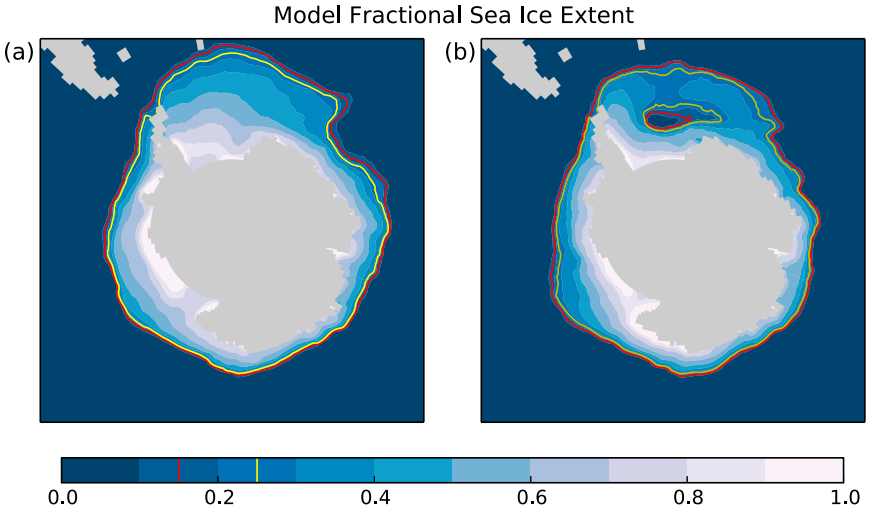

FIG. 4. Annual-mean Antarctic fractional sea ice extent in the model in (a) a year without a polynya and (b) a year with a polynya. The red and yellow contours denote 0.15 and 0.25 fractional ice extents, respectively.

because the polynyas do not occur in the same location each time. Instead, annual-mean fractional sea ice extent maps from singular nonpolynya and polynya years are shown (Figs. 4a and 4b, respectively).

During a polynya year (Fig. 4b), fractional ice extent in the Weddell Sea is strongly reduced compared to a nonpolynya year (Fig. 4a). A large portion of the region has a fractional sea ice extent of 0.25 or less (Fig. 4b, yellow contour). The calculated polynya area within the 0.15 ice extent contour in Fig. 4b is 2.23×10^5 km^2, which is similar in size to that of the observed Weddell Polynya estimates (Carsey 1980; Martinson et al. 1981; Gordon et al. 2007). The eastern edge of the 0.25 ice extent contour occurs near Maud Rise, consistent with the hypothesis that the polynya formed near the seamount and was advected west by the Weddell Gyre (Gordon 1978; Holland 2001; de Steur et al. 2007). In years with polynyas, model polynya durations are also similar to that of the Weddell Polynya, which remained open for the entire winter during each year it occurred (Martinson et al. 1981). The model polynyas are also winter persistent, with most remaining open for 2 to 4 months during each year they occur.

b. *Weddell Sea changes*

Prior to polynya onset, warm, salty water collects between 500 and 3000 m in the Weddell Sea (Fig. 5). Heat (Fig. 5a) and salt (Fig. 5b) from North Atlantic Deep Water (NADW) and Circumpolar Deep Water (CDW) collect until the surface waters become dense enough, through cooling and brine rejection, to destabilize the water column. As the dense surface water sinks it entrains the warmer, saltier water from below, acting to homogenize the subsurface waters. Within this homogenized column, the surface is anomalously warm and salty and the subsurface is anomalously cold and fresh (Fig. 5; years 0 to 15) relative to the stratified mean state. The increased surface temperature allows the polynya region to remain ice free. Exposure of the surface water to wintertime atmospheric conditions results in large sensible heat losses that cause cooling and sinking. As the colder water sinks, it is replaced at the surface by warmer waters from below, thus maintaining convection.

Polynya convection ceases when the heat at depth has been depleted and a cap of freshwater from ice melt forms at the surface that stabilizes the water column. After shutoff, the surface cools and freshens, while the subsurface warms and becomes saltier (Fig. 5; years 15 to 45). Both parts of the water column relax toward their respective prepolynya states. We will refer to this relaxation as the ''recovery'' or the ''recovery period'' to distinguish it from the time period when the polynya is perturbing the deep water.

c. *Global changes*

1) PRERECOVERY

The polynya forms AABW that subsequently spreads into the Southern Ocean and South Atlantic. As the perturbation spreads outward, the time of maximum volume transport is delayed due to the increasing distance. In regions 1 and 2 (Fig. 6, inset), the maximum volume transport occurs around years 18 and 25, respectively. It takes approximately 32 yr before the volume transport reaches a maximum in region 3. The

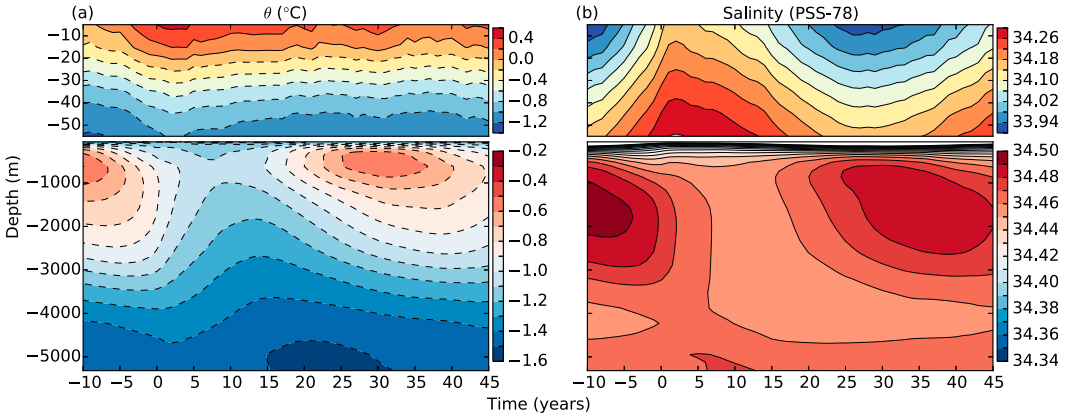

FIG. 5. Annually and spatially averaged (a) potential temperature and (b) salinity for the cooling composite. The averaging region is the same as in Fig. 1b. (top) The surface (0–50 m) is separated from the (bottom) subsurface (>50 m) and covers a smaller vertical range. Potential temperature contours are 0.2° and 0.1°C for the top and bottom panels, respectively. Salinity contours in the upper panel are 0.04 PSS-78 and 0.01 PSS-78 in the lower panel.

transport amplitudes (Fig. 6) diminish with increasing region size because the polynya water mixes and detrains into lighter density classes.

The largest anomalous volume transport out of region 1 (Fig. 6, inset) for the cooling composite polynya is approximately 2.3 Sverdrups (Sv; $1\,\text{Sv} \equiv 10^6\,\text{m}^3\,\text{s}^{-1}$). Gordon et al. (2007) calculate a 1.6–3.2-Sv convective overturning rate for the Weddell Polynya. Assuming that most of the dense waters created in the Weddell Polynya were able to leave the Weddell Sea, this convective overturning would translate to an outward volume transport of similar magnitude and is comparable to our 2.3-Sv estimate.

Deep and bottom water spreading pathways are described in Reid (1986, 1989, 1994, 1997, 2003), on which we base our description of the polynya signal spreading given below. The polynya signal spreads north and east out of the Weddell Sea (Fig. 7), expanding via pathways similar to AABW (Fig. 3). It moves into the Southern Ocean basins, then to the Atlantic, Indian, and Pacific Oceans. Refer to Fig. 3 for basin names and locations. For consistency with observational measurement standards (Joyce 1991; Hood et al. 2010), signals with magnitude smaller than 0.002°C are masked. Although there are changes in the Northern Hemisphere, we have chosen to limit our region of discussion to the Southern Hemisphere, where the strongest and most robust signals occur.

Because of the cyclic nature of polynyas in the model (Fig. 1a), the calculated deep-ocean temperature changes (Fig. 7) are composed of signals from previous polynya cycles as well as the current polynya cycle that starts at year 0 (Fig. 7b). Strong spatial similarity exists between the signals at years −5 (Fig. 7a) and 40 (Fig. 7j) and is consistent with the model's average 45-yr length for a full polynya cycle. In year 0 (Fig. 7b), the only signal from the current polynya cycle is the band of cooling near 0° in the southern Weddell–Enderby basin.

Once the signal from the current polynya cycle exits the Weddell Sea (Fig. 7c), it is more difficult to determine if a signal is related to the current or a previous polynya cycle. As described below, the years given for changes in certain basins are not necessarily the years in which they would occur relative to the start of the current polynya cycle. For example, year 0 can also be viewed as approximately year 45 of the previous polynya cycle, and so on. Based on further analysis (see Figs. 9–11), we assume that signals in the South Atlantic and Southern Ocean are from the current polynya cycle unless otherwise noted. For basins in the Indian and Pacific Oceans, polynya signals are

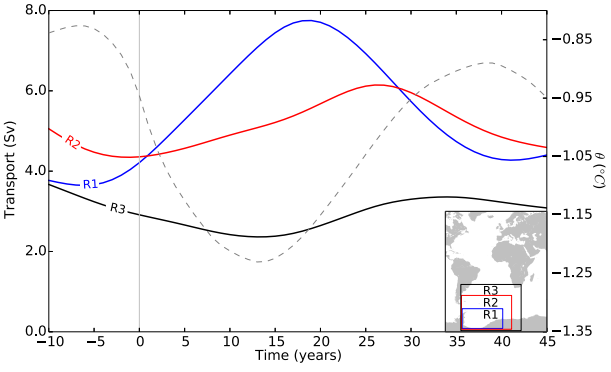

FIG. 6. Low-pass filtered annual-mean Antarctic Bottom Water ($\sigma_2 \geq 37.13\,\text{kg}\,\text{m}^{-3}$) transport out of various regions (inset) in the Weddell Sea and South Atlantic showing the transport increase associated with a polynya opening in the region. The cooling composite polynya potential temperature from Fig. 2a has been included for reference (dashed line). The vertical gray bar denotes the zero year. A Butterworth filter with a cutoff frequency of $0.1\,\text{yr}^{-1}$ has been applied.

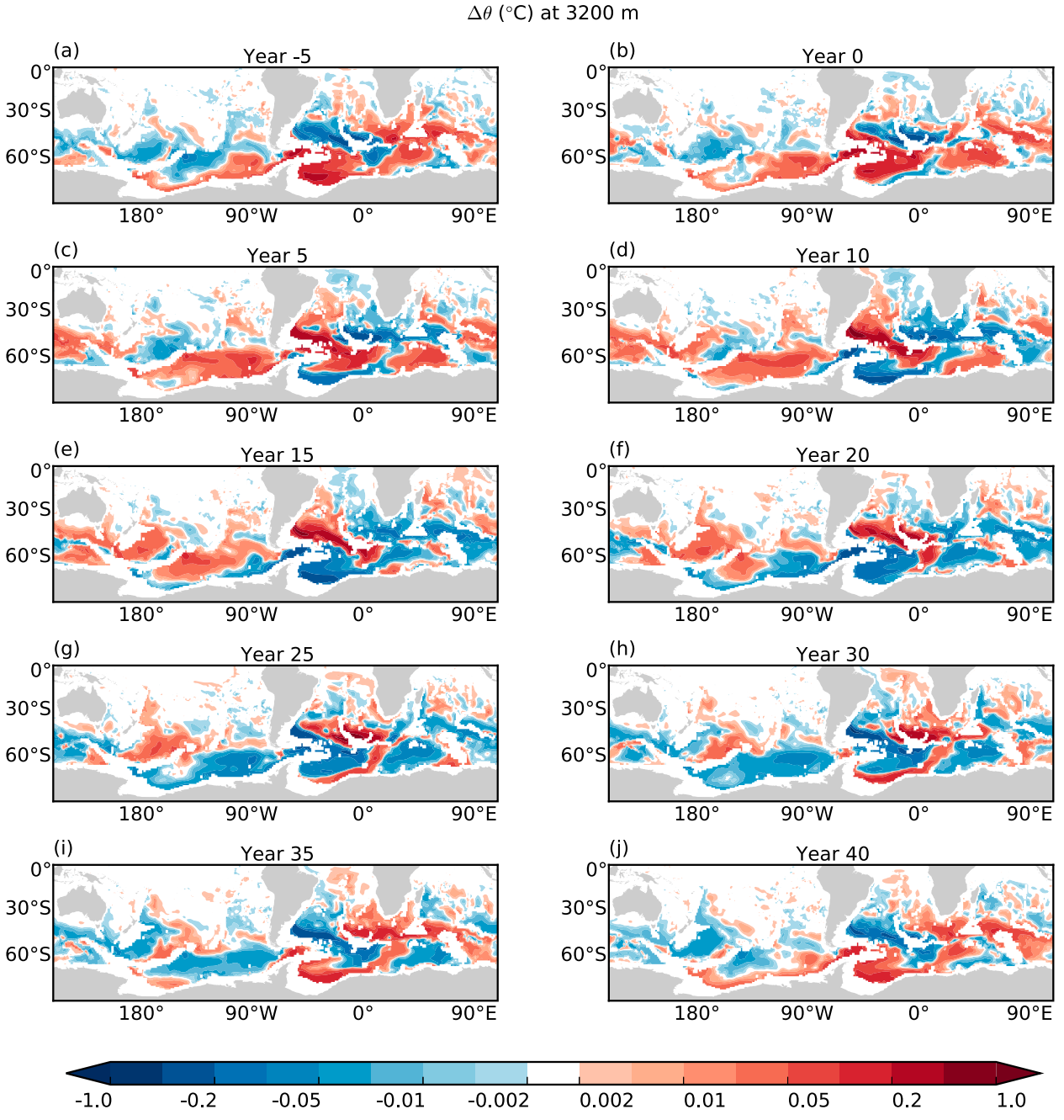

FIG. 7. Temperature anomalies relative to the long-term mean of the cooling composite showing prepolynya warming, polynya cooling, and the beginning of the recovery. Snapshots are at 5 yr before the zero year, the zero year, and 5, 10, 15, 20, 25, 30, 35, and 40 yr after the zero year.

probably from previous polynya cycles. For clarity, years referenced to signals from previous polynya cycles appear in single quotes.

(i) Southern Ocean

The signal appears in the Weddell–Enderby basin in year 5 (Fig. 7c) as a cooling of approximately −0.5°C. From there it continues north into the Argentine basin. The signal also propagates eastward in the Weddell–Enderby basin toward the Indian Ocean along the southern boundary of the Southwest Indian Ridge. Near the Prince Edward Fracture Zone (~46°S, 35°E), the signal appears to branch north into the Agulhas basin, but it is indistinguishable from a cooling signal that

began in this region between year −5 (Fig. 7a) and year 0 (Fig. 7b). The signal also continues eastward along the northern side of Conrad Rise (Fig. 7c; small, isolated region of white near 53°S, 41°E) and into the Crozet basin. From the Crozet basin the signal travels east, passing north of the Kerguelen Plateau and entering the Australian–Antarctic basin, and travels south, where it recirculates in the Enderby basin. A region of strong cooling of −0.1° to −0.05°C persists in the northern part of the Enderby basin around Conrad Rise from years 20 to 30 (Figs. 7f–h). In the Australian–Antarctic basin, cooling of a similar magnitude appears along the Southeast Indian Ridge (~80°E) between years 15 to 25 (Figs. 7e–g), with the entire basin cooling around year 25. However, further analysis will show that the polynya signal in this basin is likely the result of a previous polynya cycle, at least when averaged volumetrically below 4200 m.

A component of the polynya signal also spreads westward into the Amundsen–Bellingshausen basin from the Weddell Sea. This pathway is the result of a boundary current that develops in the wake of Kelvin waves propagating from the polynya. Characteristic of Kelvin waves in the Southern Hemisphere, the signal moves around Antarctica with the continental boundary on its left. As the signal advances, it can be seen as a band of cooling of as much as −0.5°C along the southern boundary of the Amundsen–Bellingshausen basin in years 10 and 15 (Figs. 7d and 7e, respectively). By year 25 (Fig. 7g), most of this basin exhibits cooling. Maximum cooling of −0.2°C occurs in the southeastern Amundsen–Bellingshausen basin in the same year.

(ii) Atlantic Ocean

The Atlantic basins are fed directly from the Weddell–Enderby basin. The polynya signal enters the Argentine basin via a boundary current that follows the eastern edge of the South Sandwich Fracture Zone (Figs. 7d–f). Maximum cooling of −0.5°C occurs in the Argentine basin around year 25 (Fig. 7g). At the same time, the signal enters the Brazil basin through the Vema and Hunter Channels, having continued north along the South American continental margin. From the Brazil basin it continues northward, then eastward into the Angola basin via the Romanche Fracture Zone (not shown).

(iii) Indian Ocean

In the western Indian Ocean basins, the polynya signal enters the Crozet basin from the Weddell–Enderby basin. It continues north into the Madagascar–Mascarene basin and later into the Somali basin. Cooling of approximately −0.02°C occurs along the east coast of Madagascar in years '25' (Fig. 7g) and '30' (Fig. 7h). Part of the signal that reaches the Crozet basin is also transported eastward via the Antarctic Circumpolar Current (ACC), mostly passing north of the Kerguelen Plateau and entering the Australian–Antarctic basin. Via the Australian–Antarctic basin, the polynya signal arrives in the eastern Indian Ocean basins. It first enters the South Australian basin (Fig. 7f), continues north to the Wharton basin in year '25' (Fig. 7g), and finally spreads into the mid-Indian basin. In most of these basins, maximum cooling ranges between −0.005° and −0.02°C.

(iv) Pacific Ocean

The Pacific Ocean basins have a more complicated structure because the polynya signal enters from the west via the Indian Ocean and/or the east via Drake Passage. From the east, the signal enters the southwest Pacific basin and some of the eastern peripheral basins, such as the Chile–Roggeveen basin, from the Amundsen–Bellingshausen basin. From the west, the signal enters the Tasman basin, and the southwest Pacific basin again, from both the Australian–Antarctic and South Australian basins. The signal in the southwest Pacific basin is visible as a thin band of cooling of about −0.01°C along its western boundary (Fig. 7g). From years '30' to '40' (Figs. 7h–j), this band of cooling thickens and penetrates deeper into the basin, until nearly the entire basin exhibits cooling between −0.02° and −0.005°C in year '40' (Fig. 7j).

2) RECOVERY

Here we present changes during the recovery period, first at various depths from the surface to the bottom (Fig. 8) and then as abyssal basin averages below 4200 m (Fig. 9). Salinity is reported on the dimensionless 1978 Practical Salinity Scale (PSS-78). It is useful to recall that the recovery changes manifest themselves differently in the surface and subsurface oceans. The surface recovery is generally characterized by cooling and freshening and the subsurface recovery is characterized by warming and salinification. In the subsurface ocean, density changes (not shown) are dominated by temperature changes. In many regions, density changes resulting from temperature changes are partially compensated by density changes resulting from salinity changes.

In the surface ocean (Figs. 8a,b), cooling and freshening signals occur south of 30°N. A few small, isolated regions are found north of about 30°N (not shown) in the Pacific and Atlantic Oceans, but the majority of the cooling and freshening is confined to the South Atlantic and Southern Ocean. Temperature and salinity changes typically range from −0.1° to −1.0°C and −0.1 to −1.0, respectively.

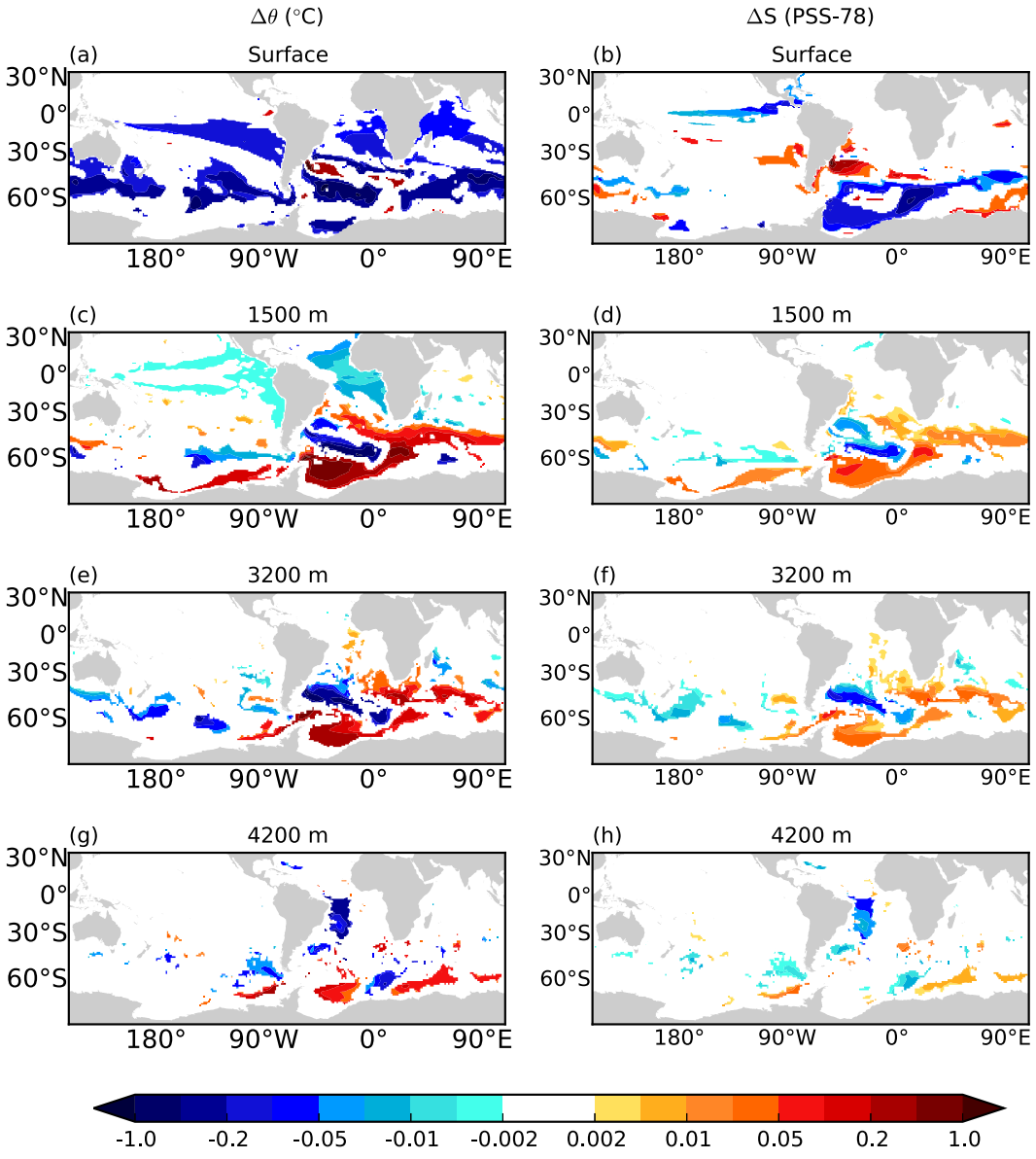

FIG. 8. Temperature and salinity changes at the surface, 1500 m, 3200 m, and 4200 m calculated from the warming composite. Differences are calculated using the decadal mean centered at the time of the maximum temperature minus the decadal mean centered at the time of the minimum temperature after the zero year (Fig. 2b). All values are significant from zero at the 95% confidence level based on the Student's *t* distribution.

In contrast to the surface ocean cooling and freshening, the subsurface predominantly exhibits warming and salinification, particularly in the Weddell, Enderby, Cape, and Agulhas basins. At 1500 m (Figs. 8c,d), warming between 0.01° and 1.0°C occurs in the Weddell Sea and to the north and east in the Cape and Agulhas basins and north of Kerguelen Plateau. Salinity increases follow similar patterns with values ranging from 0.002 to 0.1.

At 3200 m (Figs. 8e,f), the spatial structures of the temperature and salinity changes are similar to each other. The influence of topographic steering is obvious at this depth. Positive temperature and salinity changes are confined to the Antarctic continental margin between 60° and 90°W, resulting from boundary currents developed in the wake of topographic Rossby waves and Kelvin waves. Warming ranges from 0.005° to 0.5°C, and an increase in salinity of 0.002 to 0.05 occurs.

At 4200 m (Figs. 8g,h), warming and salinification occur in the Weddell–Enderby basin, along the southwestern margin of the Australian–Antarctic basin, and

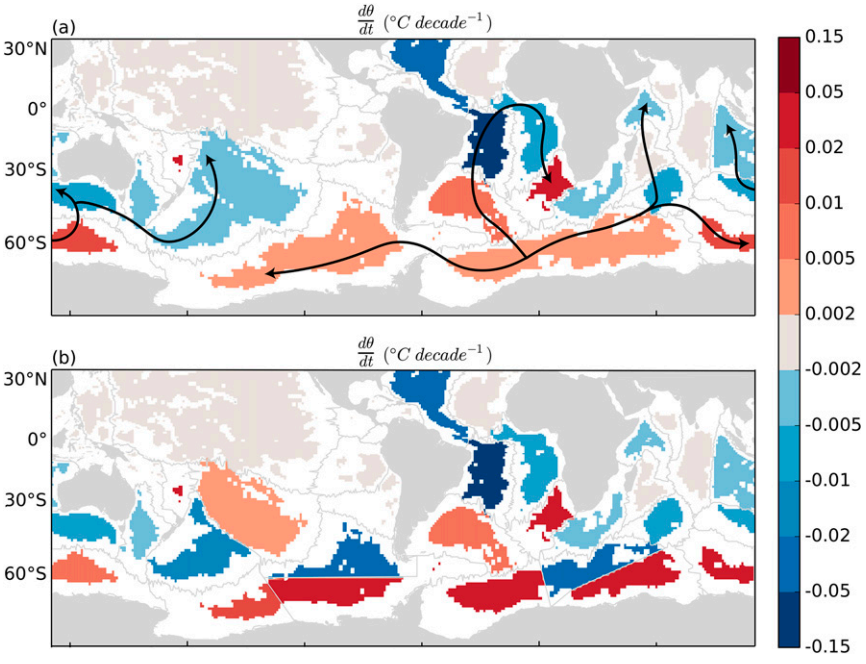

FIG. 9. Basin-mean warming rates (°C decade^{-1}) averaged below 4200 m for the warming composite. (a) Black arrows depict the basin-to-basin polynya signal spreading pathways. (b) The Weddell–Enderby, Australian–Antarctic, Amundsen–Bellingshausen, and southwest Pacific basins have been split into subsections. Decadal warming rates are calculated by averaging the yearly rates of basin-mean temperature change over years 8 to 18 and multiplying by 10. Basin boundaries are as in Purkey and Johnson (2010), with the exception of the subsections. Gray shaded basins exhibit temperature changes less than 0.002°C decade^{-1}. Bathymetry shallower than 4200 m appears white.

along the southeastern margin of the Amundsen–Bellingshausen basin. These signals range from 0.01° to 0.2°C and 0.002 to 0.05.

Basin-mean warming below 4200 m occurs throughout the Southern Ocean between years 8 and 18 of the warming composite [Fig. 9a; analogous to years 21 to 31 of the cooling composite (Fig. 2a)]. Of the three Southern Ocean basins, the Australian–Antarctic basin exhibits the strongest warming trend at 0.019°C decade^{-1}, while the Weddell–Enderby and Amundsen–Bellingshausen basins have temperature trends of 0.002°C decade^{-1}. The Brazil, Crozet, South Australian, and southwest Pacific basins, among others, exhibit cooling that will be discussed later.

Given that the Weddell–Enderby basin is the polynya source region, it seems odd that this basin does not have the strongest warming signal. The Amundsen–Bellingshausen basin also has a relatively weak warming, while the Australian–Antarctic basin, which is far from the polynya region, experiences warming that is an order of magnitude larger than the other two basins. However, some of the larger basins, which require more time for temperature perturbations to traverse, often contain both warming and cooling signals (Fig. 7). We analyze subsections of these basins next.

The Weddell–Enderby and Amundsen–Bellingshausen basins contain large subsections with strong cooling and warming signals (Fig. 9b). The average of these opposing temperature signals results in a weak warming in both basins (Fig. 9a). Alone, the Weddell basin exhibits a 0.032°C decade^{-1} warming trend (Fig. 9b). This is an order of magnitude larger than that for the Weddell–Enderby basin (Fig. 9a) and is consistent with our supposition that basins in close proximity to the polynya source region should exhibit strong warming during their recovery.

Each basin (Fig. 10, Table 1) exhibits a time lag that varies in magnitude depending on 1) its proximity to the Weddell Sea and/or 2) how quickly signals from the Weddell Sea can reach it. Water from the polynya adheres to the spreading pathways of deep and bottom waters outlined in Fig. 9a. This explains the increasing lag of the polynya signal from the Weddell basin to the Argentine, Brazil, Angola, and Cape basins (Fig. 10a), for example, and also why some basins exhibit cooling (Fig. 9). In the Cape basin, this lag is so long that the basin-mean temperature does not begin decreasing from the polynya signal until approximately year 30 (Fig. 10a), which is at the end of the decade over which temperature changes are calculated for Fig. 9. We

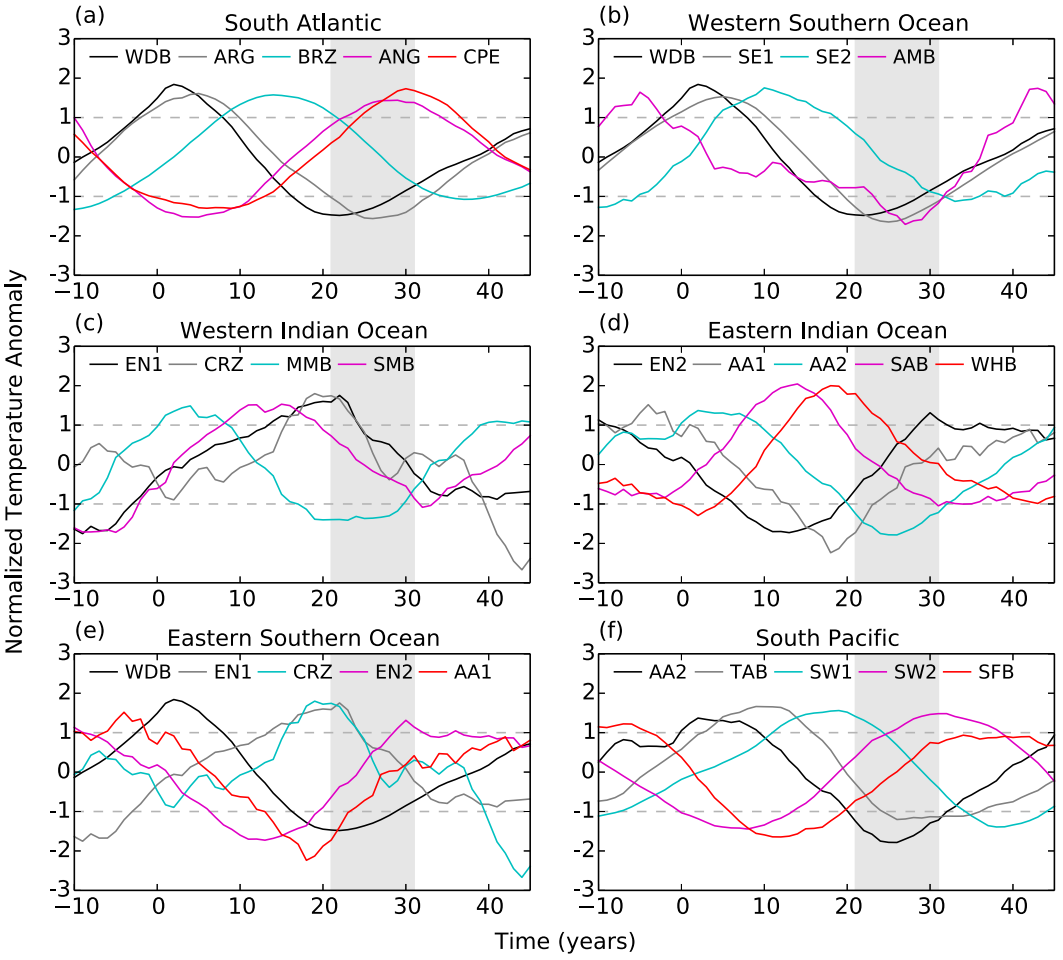

FIG. 10. Time series of normalized basin-mean temperature anomalies over the time of the cooling composite in (a) South Atlantic, (b) western Southern Ocean, (c) western Indian Ocean, (d) eastern Indian Ocean, (e) eastern Southern Ocean, and f) South Pacific. Basin time series have been grouped according to the spreading pathways in Fig. 9a. Dashed black horizontal lines denote ±1 temperature anomaly standard deviation. Values of the temperature anomaly standard deviation for each basin are provided in Table 1. The gray rectangle in each plot shows the time period over which the basin-mean temperature trends were calculated for Fig. 9. Refer to Fig. 3 for basin locations.

deduce that the strong warming in the Cape basin (Fig. 9a; Fig. 10a, gray box) is likely the recovery warming from the previous polynya cycle.

The Cape basin is not unique in this respect; many basins are experiencing warming or cooling from a previous polynya cycle (Fig. 9; summarized in Fig. 11). To distinguish between basins affected by the current polynya and those affected by previous polynya cycles, we use Fig. 10 as a method for establishing causality. The spreading pathways in Fig. 9a are critical for determining which polynya cycle is affecting a given basin. The following assumptions are also necessary: 1) any basin that exhibits at least 10 yr of cooling beginning before the zero year (Fig. 10) is assumed to be cooling from a previous polynya cycle, and 2) any basin that is further along the spreading pathway(s) from the basins determined in 1 must also be experiencing the effects of a previous polynya cycle. Based on these criteria, the following basins are experiencing effects of the current polynya cycle: the Weddell basin (WDB), Argentine basin (ARG), Brazil basin (BRZ), Angola basin (ANG), the southeast Pacific basin (SE1 and SE2), the first part of the Enderby basin (EN1), and the Crozet basin (CRZ). All other basins are experiencing warming or cooling from at least one polynya cycle prior.

By accounting for previous polynya cycles we can estimate the time when warming will begin in each basin relative to the current polynya cycle (Fig. 11). The year when warming begins in each basin tends to be larger further along each spreading pathway and hence illustrates the polynya signal spreading.

TABLE 1. Standard deviations of basin-mean temperature anomalies for each basin in Fig. 10, calculated as anomalies from the long-term mean of basin-mean temperature. Refer to Fig. 3 for basin locations.

Basin	Standard deviation (°C)
WDB	0.035
EN1	0.022
EN2	0.014
ARG	0.024
BRZ	0.068
ANG	0.006
CPE	0.029
CPE	0.028
SE1	0.044
SE2	0.017
AMB	0.013
CRZ	0.005
MMB	0.009
SMB	0.002
AA1	0.015
AA2	0.013
SAB	0.005
WHB	0.002
TAB	0.007
SW1	0.010
SW2	0.004
SFB	0.016

Comparison of maximum basin-mean warming rates (°C decade^{-1}) (Fig. 11) shows the strength and spatial extent of the polynya recovery signal, which generally decreases with increasing distance from the Weddell Sea. The strongest signals occur in the South Atlantic and the Southern Ocean (Fig. 11). In some basins, such as the North Pacific basin, the maximum warming rate never exceeds 0.002°C decade^{-1}. In the North Atlantic basins (not shown), polynya-induced changes are difficult to distinguish from changes arising from internal variability such as AMOC fluctuations. We cannot be certain that changes in these basins are related to the polynya without further analysis.

4. Discussion

a. Dynamics

The structure of the temperature and salinity patterns is related to the polynya signal dynamics. The dynamics are categorized in two parts: 1) the wavelike signal that acts on shorter time scales and 2) the advective/diffusive signal that acts on longer time scales. The fast signal propagated by planetary waves (Kawase 1987; Hallberg and Rhines 1996; Kawano et al. 2010; Masuda et al. 2010; Hirabara et al. 2012; Latif et al. 2013; Martin et al. 2013) allows impacts of the polynya to be felt far from the Weddell Sea relatively quickly, on the order of 50 yr or less (Nakano and Suginohara 2002). Kelvin waves and topographic Rossby waves are potentially responsible (Hallberg and Rhines 1996). The waves also set up boundary currents in their wake. These currents, along with the general ocean circulation, advect the polynya signal, giving rise to changes on longer time scales.

b. Timing

Considerable time passes before polynya-induced changes reach remote regions. The polynya signal experiences a time lag according to the spreading pathways of deep and bottom water out of the Weddell Sea (Fig. 10). Thus, the polynya recovery in successive basins along the spreading pathways occurs with a time lag as well (Fig. 11). For example, the recovery begins around year 22 in the Weddell basin, year 26 in the Argentine basin, and year 35 in the Brazil basin (Figs. 10a, 11). In many basins, particularly those further away from the Weddell Sea or those blocked by large topographic features, the changes that occur are likely the result of previous polynya cycles.

Changes resulting from the current polynya occur in the South Atlantic and the Southern Ocean (Fig. 11). The Argentine basin is warming due to the recovery from the current polynya, while the Brazil and Angola basins are cooling from the current polynya. The Cape basin has yet to begin cooling from the current polynya and instead appears to be experiencing a recovery from the previous polynya cycle. Although not shown as a pathway in Fig. 9a, deep and bottom waters also enter the Cape basin from the south. These waters leave the Weddell–Enderby basin through gaps in the Southwest Indian Ridge and spread into the Agulhas and Cape basins (Mantyla and Reid 1995). Despite this second pathway into the Cape basin, the lag of the polynya signal in the Cape basin relative to the Weddell basin (Fig. 10a) is still large (~28 yr). Analysis of the Agulhas basin time series of normalized temperature anomalies (not shown) reveals that it too has a lag (relative to the Weddell basin) of length similar to that of the Angola basin relative to the Weddell basin (Fig. 10a; ~25 yr). Both the Angola basin and Agulhas basin time series reach their normalized temperature anomaly maxima slightly before the Cape basin. This may indicate that the polynya signal enters the Cape basin from both the Agulhas and Angola basins. It could also explain the strong maximum warming rate in the Cape basin (Fig. 11) despite that both the Angola and Agulhas basins experience weaker maximum warming rates.

In the Southern Ocean, all three deep basins exhibit warming. The Australian–Antarctic basin warming (Fig. 9a) is likely due to recovery from the previous polynya cycle. When split into subsections (Figs. 9b, 10), parts

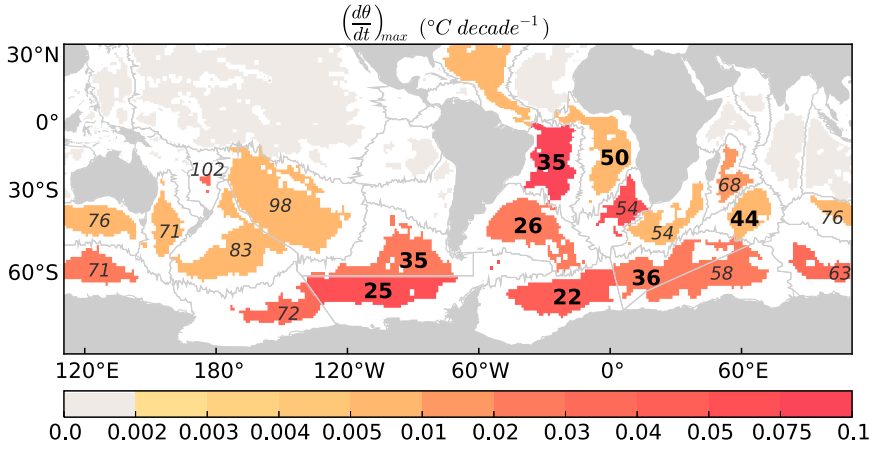

FIG. 11. Maximum basin-mean warming rates (°C decade^{-1}; color shading) for basins in Figs. 9b and 10. A 10-yr running mean is used to calculate mean warming rates for each basin time series. The largest warming rate is chosen and multiplied by 10 to obtain the decadal rate. The bold and italic numbers are the estimated time elapsed (yr) between the beginning of cooling in the Weddell Sea and the beginning of warming in each basin. Bold values indicate basins experiencing changes due to the current polynya cycle, while values in italics indicate basins experiencing changes from previous polynya cycles. Gray shaded basins have maximum warming rates less than 0.002°C decade^{-1}. Bathymetry shallower than 4200 m appears white.

of the Weddell–Enderby and Amundsen–Bellingshausen basins also appear to be experiencing recovery from the previous polynya cycle, although most of the changes in these two basins are attributable to the current polynya.

c. *Comparison to observations*

The basin-mean warming patterns in the deep-ocean model layers are similar to those in Fig. 8 of Purkey and Johnson (2010). Strong warming occurs in the abyssal Southern Ocean basins and in the Argentine basin. The basin-mean temperature changes (Fig. 9a) occur 21–31 yr after the model polynya onset, consistent with warming observed in recent studies (Johnson and Doney 2006; Johnson et al. 2007, 2008; Purkey and Johnson 2010, 2013). Most of the observations in these studies come from the 1990s and 2000s, roughly 20–30 yr after the occurrence of the observed Weddell Polynya. As reported in Purkey and Johnson (2010), the mean and median times between the initial and final repeat section occupations were 12.9 and 11.9 yr, respectively. We also calculated basin-mean salinity changes for the same period (not shown), but for nearly every basin the changes were smaller than standard 0.002 PSS-78 measurement precision (Joyce 1991; Hood et al. 2010). We do not discuss them further.

With the exception of the Australian–Antarctic basin, we restrict our comparison to basins that are warming as a result of the current polynya recovery. Evidence suggests there could have been large Weddell Sea polynyas prior to the 1970s (Goosse et al. 2009; Meier et al. 2013). Consequently, we include the Australian–Antarctic warming. Our calculations are summarized in Table 2. The calculated warming rates in the Weddell–Enderby, Australian–Antarctic, Amundsen–Bellingshausen, and Argentine basins are 0.002°, 0.019°, 0.002°, and 0.009°C decade^{-1}, respectively.

Comparing these values with the temperature changes observed by Purkey and Johnson (2010) yields an estimate of the fractional warming that could be due to the Weddell Polynya(s) (Table 2). The current polynya recovery explains about 6% ± 11% of the warming in the Weddell–Enderby basin, 7% ± 15% in the Amundsen–Bellingshausen basin, and 33% ± 14% in the Argentine basin. The previous polynya recovery explains 34% ± 13% of the warming in the Australian–Antarctic basin. To estimate the percentage of polynya-induced warming in the abyssal Southern Ocean, we calculate the volume-weighted average warming rate of the three Southern Ocean basins (Table 2). Up to 10% ± 8% of the observed warming in the abyssal Southern Ocean in the 1990s and 2000s could be the result of the recovery from the Weddell Polynya. This percentage should be taken as an upper bound for the Southern Ocean basins because warming in the Australian–Antarctic basin is likely a result of the recovery from the previous polynya cycle. If we assume that there is no contribution from the Australian–Antarctic basin, the recovery from the polynya explains about 6% ± 8% of the observed Southern

TABLE 2. Modeled basin-mean decadal warming rates below 4200 m roughly corresponding to the period between the mid-1990s and mid-2000s (about 20–30 yr after the Weddell Polynya). Percentages of observed warming are calculated by dividing the modeled basin-mean warming rates (and their standard deviations) by observed basin-mean warming rates from Purkey and Johnson (2010). To calculate the observed basin-mean decadal warming rates we take the yearly basin-mean warming rates from Purkey and Johnson (2010) and multiply them by 10. The total Southern Ocean warming rate is calculated by volume averaging the warming rates for the Weddell–Enderby, Australian–Antarctic, and Amundsen–Bellingshausen basins. Modeled basin-mean standard deviations are determined by the differences between individual polynya basin-mean warming rates and the warming composite basin-mean warming rates. Warming percentages are not provided for subsections of the Southern Ocean basins because Purkey and Johnson (2010) provide data that have already been transformed into basin-mean estimates.

Region or basin	Mean $d\theta/dt$ (°C decade^{-1}) below 4200 m (plus or minus one standard deviation)	Percentage of observed warming (plus or minus one standard deviation)
South Atlantic basins		
Argentine basin	0.009 (±0.004)	33 (±14)
Southern Ocean basins		
Weddell–Enderby basin	0.002 (±0.004)	6 (±11)
Weddell basin	0.032 (±0.002)	—
Enderby 1	−0.038 (±0.006)	—
Enderby 2	0.028 (±0.007)	—
Amundsen–Bellingshausen basin	0.002 (±0.003)	7 (±15)
Southeast Pacific 1	0.032 (±0.005)	—
Southeast Pacific 2	−0.024 (±0.003)	—
Amundsen basin	0.017 (±0.007)	—
Australian–Antarctic basin	0.019 (±0.007)	34 (±13)
Australian–Antarctic 1	0.034 (±0.009)	—
Australian–Antarctic 2	0.009 (±0.009)	—
Total Southern Ocean	0.003 (±0.002)	10 (±8)
With no change in Australian–Antarctic basin	0.002 (±0.002)	6 (±8)

Ocean warming. This calculation assumes that the basin-mean temperature standard deviation remains the same in the Australian–Antarctic basin.

Cooling occurs in the Brazil and Angola basins, suggesting that the current polynya signal has reached these basins but that the recovery has not yet begun. If we assume that the timing of polynya-induced abyssal ocean changes is correct in our model, we would not expect Weddell Polynya signals in these basins to contribute to observed mid-1990s to mid-2000s warming, but they could contribute to the observed warming after this period. Warming in the Vema Channel and Brazil basin has been observed since the early to mid-1990s (e.g., Zenk and Morozov 2007; Purkey and Johnson 2010), the timing of which is analogous to years 15–20 of the cooling composite. During these model years, the Brazil basin is cooling. According to the timing of changes in the model, we would expect polynya cooling in the Brazil basin to reduce a warming signal that is already present. However, once the recovery starts, polynya warming in the Brazil basin would amplify the already-present warming signal. Johnson et al. (2014) find that abyssal Brazil basin warming continued between 2005 and 2014. These years are analogous to years 30–40 of the cooling composite, during which time the model Brazil basin begins warming. It is possible that some of the observed Brazil basin warming from 2005 onward is a result of the Weddell Polynya recovery.

5. Conclusions

Abyssal ocean temperature and salinity changes following cessation of a composite Weddell Sea polynya in GFDL's coupled climate model CM2G were analyzed. Two composites were constructed to quantify deep-ocean warming that occurred during the recovery period. Below 4200 m, we found patterns of deep basin warming similar but of smaller magnitude than that reported in Purkey and Johnson (2010). The strongest warming signals occurred in the South Atlantic and Southern Ocean basins and tended to decay with distance from the Weddell Sea. In the abyssal Southern Ocean basins, warming rates between 0.002° and 0.019°C decade^{-1} occurred during a 10-yr period of the recovery. Comparison to Purkey and Johnson (2010) suggests that the Weddell Polynya recovery could explain 10% ± 8% of the warming observed in the abyssal Southern Ocean. However, warming in the Australian–Antarctic basin does not appear to be from the current polynya cycle. With the Australian–Antarctic basin contribution excluded, the Weddell Polynya could explain 6% ± 8% of observed abyssal Southern Ocean

warming. The percentage contribution varies from basin to basin and is as high as 34% ± 13% for the Australian–Antarctic basin and 33% ± 14% for the Argentine basin. Percentages for the Weddell–Enderby and Amundsen–Bellingshausen basins are 6% ± 11% and 7% ± 15%, respectively.

Cooling occurred in the Brazil and Angola basins, suggesting that the current polynya signal reached these basins but that the recovery had not yet begun. Therefore, we do not expect Weddell Polynya signals in these basins to have contributed to observed mid-1990s to mid-2000s warming, but they could do so after this period. It is possible that some of the observed Brazil basin warming from 2005 onward (Johnson et al. 2014) is a result of the Weddell Polynya recovery.

Northern Hemisphere basin changes were not analyzed because the polynya signal was not discernible from internal variability. Polynya signals are capable of reaching these remote basins in fewer than 50 yr via planetary waves (Kawase 1987; Nakano and Suginohara 2002; Purkey and Johnson 2010; Hirabara et al. 2012). Recent studies indicate that both deep convection and deep-ocean temperature changes around Antarctica could impact the Northern Hemisphere, in particular the North Atlantic, via changes to the Atlantic meridional overturning circulation (AMOC) (Martin et al. 2013, 2015; Patara and Böning 2014). Further exploration of the polynya signal propagation may help explain changes in Northern Hemisphere basins.

It is clear that the 1970s Weddell Polynya impacted the abyssal oceans. Our model analysis emphasizes the importance of understanding these transient features, particularly their spatial structure and the time scales on which they act. Composite analysis has proven to be a useful tool for studying the polynyas, but even with composites of over 30 polynyas, variability between individual events complicated signal analysis. Differences in event length, magnitude, and the spatiotemporal influence of the polynyas often combined so that the composite signal robustness was reduced. This limited our analysis to broad, large-scale mean changes. To overcome these issues, we plan to investigate the effects of inter-polynya variability by regularly forcing large polynyas in the Weddell Sea. Control over the timing of the polynyas could help differentiate between changes caused by the current polynya cycle and those caused by previous polynya cycles.

Because the polynya recovery manifests itself as a warming signal in deep and bottom waters, distinguishing between this signal and that of anthropogenic climate change requires accurate modeling of polynya dynamics. Our study employs a single model to investigate open-ocean polynyas, so the results are tied to the particular realization of ocean dynamics within the model. Heuzé et al. (2015) indirectly investigate the effects of ocean-open polynyas across CMIP5 models by examining bottom property changes resulting from reduced open-ocean convection under anthropogenic climate change. However, their study seeks to understand the impacts resulting from models creating AABW through open-ocean convection (and not through shelf processes; Heuzé et al. 2013) rather than a comparison of open-ocean polynya dynamics and effects. Besides Heuzé et al. (2015), we can find no comprehensive study in which impacts related to open-ocean convection are compared across models. Multimodel studies investigating polynya effects could be beneficial for understanding the sensitivity of polynya signals to model characteristics such as resolution, background diffusivity, and overflow parameterizations.

Acknowledgments. The authors thank Sonya Legg, Adele Morrison, Stephen Griffies, Robert Key, and two anonymous reviewers for providing valuable feedback that greatly improved this manuscript. We thank Sarah G. Purkey for providing observed basin-mean temperature rates on isobars and basin boundary coordinates, which facilitated comparison between our model and the observations. Figures were created using Python's Matplotlib plotting package. Hannah Zanowski was supported under Awards NA08OAR4320752 and NA14OAR4320106 from the National Oceanic and Atmospheric Administration, U.S. Department of Commerce. The statements, findings, conclusions, and recommendations are those of the author(s) and do not necessarily reflect the views of NOAA or the U.S. Department of Commerce.

REFERENCES

Adcroft, A., and R. Hallberg, 2006: On methods for solving the oceanic equations of motion in generalized vertical coordinates. *Ocean Modell.*, **11**, 224–233, doi:10.1016/j.ocemod.2004.12.007.

Anderson, J. L., and Coauthors, 2004: The new GFDL global atmosphere and land model AM2–LM2: Evaluation with prescribed SST simulations. *J. Climate*, **17**, 4641–4673, doi:10.1175/JCLI-3223.1.

Carmack, E. C., and T. D. Foster, 1975a: Circulation and distribution of oceanographic properties near the Filchner Ice Shelf. *Deep-Sea Res. Oceanogr. Abstr.*, **22**, 77–90, doi:10.1016/0011-7471(75)90097-2.

——, and ——, 1975b: On the flow of water out of the Weddell Sea. *Deep-Sea Res. Oceanogr. Abstr.*, **22**, 711–724, doi:10.1016/0011-7471(75)90077-7.

Carsey, F. D., 1980: Microwave observation of the Weddell Polynya. *Mon. Wea. Rev.*, **108**, 2032–2044, doi:10.1175/1520-0493(1980)108<2032:MOOTWP>2.0.CO;2.

Coles, V. J., M. S. McCartney, D. B. Olson, and W. M. Smethie Jr., 1996: Changes in Antarctic Bottom Water properties in the

western South Atlantic in the late 1980s. *J. Geophys. Res.*, **101**, 8957–8970, doi:10.1029/95JC03721.

Comiso, J. C., and A. L. Gordon, 1987: Recurring polynyas over the Cosmonaut Sea and the Maud Rise. *J. Geophys. Res.*, **92**, 2819–2833, doi:10.1029/JC092iC03p02819.

——, and ——, 1996: Cosmonaut polynya in the Southern Ocean: Structure and variability. *J. Geophys. Res.*, **101**, 18 297–18 313, doi:10.1029/96JC01500.

de Lavergne, C., J. B. Palter, E. D. Galbraith, R. Bernardello, and I. Marinov, 2014: Cessation of deep convection in the open Southern Ocean under anthropogenic climate change. *Nat. Climate Change*, **4**, 278–282, doi:10.1038/nclimate2132.

de Steur, L., D. M. Holland, R. D. Muench, and M. G. McPhee, 2007: The warm water "halo" around Maud Rise: Properties, dynamics and impact. *Deep-Sea Res. I*, **54**, 871–896, doi:10.1016/j.dsr.2007.03.009.

Dunne, J. P., and Coauthors, 2012: GFDL's ESM2 global coupled climate–carbon Earth system models. Part I: Physical formulation and baseline simulation characteristics. *J. Climate*, **25**, 6646–6665, doi:10.1175/JCLI-D-11-00560.1.

Fahrbach, E., M. Hoppema, G. Rohardt, M. Schröder, and A. Wisotzki, 2004: Decadal- scale variations of water mass properties in the deep Weddell Sea. *Ocean Dyn.*, **54**, 77–91, doi:10.1007/s10236-003-0082-3.

——, ——, ——, O. Boebel, O. Klatt, and A. Wisotzki, 2011: Warming of deep and abyssal water masses along the Greenwich meridian on decadal time scales: The Weddell Gyre as a heat buffer. *Deep-Sea Res. II*, **58**, 2509–2523, doi:10.1016/j.dsr2.2011.06.007.

Foster, T. D., and E. C. Carmack, 1976a: Frontal zone mixing and Antarctic Bottom Water formation in the southern Weddell Sea. *Deep-Sea Res. Oceanogr. Abstr.*, **23**, 301–317, doi:10.1016/0011-7471(76)90872-X.

——, and ——, 1976b: Temperature and salinity structure in the Weddell Sea. *J. Phys. Oceanogr.*, **6**, 36–44, doi:10.1175/1520-0485(1976)006<0036:TASSIT>2.0.CO;2.

Gill, A. E., 1973: Circulation and bottom water production in the Weddell Sea. *Deep-Sea Res. Oceanogr. Abstr.*, **20**, 111–140, doi:10.1016/0011-7471(73)90048-X.

Goosse, H., and T. Fichefet, 2001: Open-ocean convection and polynya formation in a large-scale ice–ocean model. *Tellus*, **53A**, 94–111, doi:10.1034/j.1600-0870.2001.01061.x.

——, W. Lefebvre, A. de Montety, E. Crespin, and A. H. Orsi, 2009: Consistent past half-century trends in the atmosphere, the sea ice and the ocean at high southern latitudes. *Climate Dyn.*, **33**, 999–1016, doi:10.1007/s00382-008-0500-9.

Gordon, A. L., 1978: Deep Antarctic convection west of Maud Rise. *J. Phys. Oceanogr.*, **8**, 600–612, doi:10.1175/1520-0485(1978)008<0600:DACWOM>2.0.CO;2.

——, 1982: Weddell Deep Water variability. *J. Mar. Res.*, **40**, 199–217.

——, 1991: Two stable modes of Southern Ocean winter stratification. *Deep Convection and Deep Water Formation in the Oceans*, P. C. Chu and J. C. Gascard, Eds., Elsevier Oceanography Series, Vol. 57, Elsevier, 17–35, doi:10.1016/S0422-9894(08)70058-8.

——, M. Visbeck, and J. C. Comiso, 2007: A possible link between the Weddell Polynya and the southern annular mode. *J. Climate*, **20**, 2558–2571, doi:10.1175/JCLI4046.1.

Griffies, S. M., R. C. Pacanowski, and R. W. Hallberg, 2000: Spurious diapycnal mixing associated with advection in a z-coordinate ocean model. *Mon. Wea. Rev.*, **128**, 538–564, doi:10.1175/1520-0493(2000)128<0538:SDMAWA>2.0.CO;2.

Hallberg, R., and P. Rhines, 1996: Buoyancy-driven circulation in an ocean basin with isopycnals intersecting the sloping boundary. *J. Phys. Oceanogr.*, **26**, 913–940, doi:10.1175/1520-0485(1996)026<0913:BDCIAO>2.0.CO;2.

——, and A. Adcroft, 2009: Reconciling estimates of the free surface height in Lagrangian vertical coordinate ocean models with mode-split time stepping. *Ocean Modell.*, **29**, 15–26, doi:10.1016/j.ocemod.2009.02.008.

Heuzé, C., K. J. Heywood, D. P. Stevens, and J. K. Ridley, 2013: Southern Ocean bottom water characteristics in CMIP5 models. *Geophys. Res. Lett.*, **40**, 1409–1414, doi:10.1002/grl.50287.

——, ——, ——, and ——, 2015: Changes in global ocean bottom properties and volume transports in CMIP5 models under climate change scenarios. *J. Climate*, **28**, 2917–2943, doi:10.1175/JCLI-D-14-00381.1.

Hirabara, M., H. Tsujino, H. Nakano, and G. Yamanaka, 2012: Formation mechanism of the Weddell Sea Polynya and the impact on the global abyssal ocean. *J. Oceanogr.*, **68**, 771–796, doi:10.1007/s10872-012-0139-3.

Holland, D. M., 2001: Explaining the Weddell Polynya—A large ocean eddy shed at Maud Rise. *Science*, **292**, 1697–1700, doi:10.1126/science.1059322.

Hood, E. M., C. L. Sabine, and B. M. Sloyan, Eds., 2010: GO-SHIP repeat hydrography manual: A collection of expert reports and guidelines. IOCCP Rep. 14, ICPO Publication Series 134, accessed 30 July 2015. [Available online at www.go-ship.org/HydroMan.html.]

Ilicak, M., A. Adcroft, S. M. Griffies, and R. W. Hallberg, 2012: Spurious dianeutral mixing and the role of momentum closure. *Ocean Modell.*, **45-46**, 37–58, doi:10.1016/j.ocemod.2011.10.003.

Johnson, G. C., and S. C. Doney, 2006: Recent western South Atlantic Bottom Water warming. *Geophys. Res. Lett.*, **33**, L14614, doi:10.1029/2006GL026769.

——, S. Mecking, B. M. Sloyan, and S. E. Wijffels, 2007: Recent bottom water warming in the Pacific Ocean. *J. Climate*, **20**, 5365–5375, doi:10.1175/2007JCLI1879.1.

——, S. G. Purkey, and J. L. Bullister, 2008: Warming and freshening in the abyssal southeastern Indian Ocean. *J. Climate*, **21**, 5351–5363, doi:10.1175/2008JCLI2384.1.

——, K. E. McTaggart, and R. Wanninkhof, 2014: Antarctic Bottom Water temperature changes in the western South Atlantic from 1989 to 2014. *J. Geophys. Res. Oceans*, **119**, 8567–8577, doi:10.1002/2014JC010367.

Joyce, T. M., 1991: Introduction to the collection of expert reports compiled for the WHP programme. WHP Operations and Methods—July 1991, WOCE Hydrographic Programme Office Rep., 4 pp. [Available online at http://geo.h2o.ucsd.edu/documentation/manuals/pdf/91_1/introjoy.pdf.]

Kawano, T., T. Doi, H. Uchida, S. Kouketsu, M. Fukasawa, Y. Kawai, and K. Katsumata, 2010: Heat content change in the Pacific Ocean between the 1990s and 2000s. *Deep-Sea Res. II*, **57**, 1141–1151, doi:10.1016/j.dsr2.2009.12.003.

Kawase, M., 1987: Establishment of deep ocean circulation driven by deep-water production. *J. Phys. Oceanogr.*, **17**, 2294–2317, doi:10.1175/1520-0485(1987)017<2294:EODOCD>2.0.CO;2.

Latif, M., T. Martin, and W. Park, 2013: Southern Ocean sector centennial climate variability and recent decadal trends. *J. Climate*, **26**, 7767–7782, doi:10.1175/JCLI-D-12-00281.1.

Legg, S., R. W. Hallberg, and J. B. Girton, 2006: Comparison of entrainment in overflows simulated by *z*-coordinate, isopycnal and non-hydrostatic models. *Ocean Modell.*, **11**, 69–97, doi:10.1016/j.ocemod.2004.11.006.

Mantyla, A. W., and J. L. Reid, 1995: On the origins of deep and bottom waters of the Indian Ocean. *J. Geophys. Res.*, **100**, 2417–2439, doi:10.1029/94JC02564.

Martin, T., W. Park, and M. Latif, 2013: Multi-centennial variability controlled by Southern Ocean convection in the Kiel Climate Model. *Climate Dyn.*, **40**, 2005–2022, doi:10.1007/s00382-012-1586-7.

——, ——, and ——, 2015: Southern Ocean forcing of the North Atlantic at multi-centennial time scales in the Kiel Climate Model. *Deep-Sea Res. II*, **114**, 39–48, doi:10.1016/j.dsr2.2014.01.018.

Martinson, D. G., P. D. Killworth, and A. L. Gordon, 1981: A convective model for the Weddell Polynya. *J. Phys. Oceanogr.*, **11**, 466–488, doi:10.1175/1520-0485(1981)011<0466:ACMFTW>2.0.CO;2.

Masuda, S., and Coauthors, 2010: Simulated rapid warming of abyssal North Pacific waters. *Science*, **329**, 319–322, doi:10.1126/science.1188703.

Meier, W. N., D. Gallaher, and G. G. Campbell, 2013: New estimates of Arctic and Antarctic sea ice extent during September 1964 from recovered *Nimbus I* satellite imagery. *Cryosphere*, **7**, 699–705, doi:10.5194/tc-7-699-2013.

Meredith, M. P., A. C. Naveira Garabato, A. L. Gordon, and G. C. Johnson, 2008: Evolution of deep and bottom waters of the Scotia Sea, Southern Ocean, during 1995–2005. *J. Climate*, **21**, 3327–3343, doi:10.1175/2007JCLI2238.1.

Milly, P. C. D., and Coauthors, 2014: An enhanced model of land water and energy for global hydrologic and Earth-system studies. *J. Hydrometeor.*, **15**, 1739–1761, doi:10.1175/JHM-D-13-0162.1.

Moore, G. W. K., K. Alverson, and I. A. Renfrew, 2002: A reconstruction of the air–sea interaction associated with the Weddell Polynya. *J. Phys. Oceanogr.*, **32**, 1685–1698, doi:10.1175/1520-0485(2002)032<1685:AROTAS>2.0.CO;2.

Nakano, H., and N. Suginohara, 2002: Importance of the eastern Indian Ocean for the abyssal Pacific. *J. Geophys. Res.*, **107**, 3219, doi:10.1029/2001JC001065.

Orsi, A. H., G. C. Johnson, and J. L. Bullister, 1999: Circulation, mixing, and production of Antarctic Bottom Water. *Prog. Oceanogr.*, **43**, 55–109, doi:10.1016/S0079-6611(99)00004-X.

Patara, L., and C. W. Böning, 2014: Abyssal ocean warming around Antarctica strengthens the Atlantic overturning circulation. *Geophys. Res. Lett.*, **41**, 3972–3978, doi:10.1002/2014GL059923.

Purkey, S. G., and G. C. Johnson, 2010: Warming of global abyssal deep Southern Ocean waters between the 1990s and 2000s: Contributions to global heat and sea level rise budgets. *J. Climate*, **23**, 6336–6350, doi:10.1175/2010JCLI3682.1.

——, and ——, 2012: Global contraction of Antarctic Bottom Water between the 1980s and 2000s. *J. Climate*, **25**, 5830–5844, doi:10.1175/JCLI-D-11-00612.1.

——, and ——, 2013: Antarctic Bottom Water warming and freshening: Contributions to sea level rise, ocean freshwater budgets, and global heat gain. *J. Climate*, **26**, 6105–6122, doi:10.1175/JCLI-D-12-00834.1.

Reid, J. L., 1986: On the total geostrophic circulation of the South Pacific Ocean: Flow patterns, tracers, and transports. *Prog. Oceanogr.*, **16**, 1–61, doi:10.1016/0079-6611(86)90036-4.

——, 1989: On the total geostrophic circulation of the South Atlantic Ocean: Flow patterns, tracers, and transports. *Prog. Oceanogr.*, **23**, 149–244, doi:10.1016/0079-6611(89)90001-3.

——, 1994: On the total geostrophic circulation of the North Atlantic Ocean: Flow patterns, tracers, and transports. *Prog. Oceanogr.*, **33**, 1–92, doi:10.1016/0079-6611(94)90014-0.

——, 1997: On the total geostrophic circulation of the Pacific Ocean: Flow patterns, tracers, and transports. *Prog. Oceanogr.*, **39**, 263–352, doi:10.1016/S0079-6611(97)00012-8.

——, 2003: On the total geostrophic circulation of the Indian Ocean: Flow patterns, tracers, and transports. *Prog. Oceanogr.*, **56**, 137–186, doi:10.1016/S0079-6611(02)00141-6.

Robertson, R., M. Visbeck, A. L. Gordon, and E. Fahrbach, 2002: Long-term temperature trends in the deep waters of the Weddell Sea. *Deep-Sea Res. II*, **49**, 4791–4806, doi:10.1016/S0967-0645(02)00159-5.

Seabrooke, J. M., G. L. Hufford, and R. B. Elder, 1971: Formation of Antarctic Bottom Water in the Weddell Sea. *J. Geophys. Res.*, **76**, 2164–2178, doi:10.1029/JC076i009p02164.

Smedsrud, L. H., 2005: Warming of the deep water in the Weddell Sea along the Greenwich meridian: 1977–2001. *Deep-Sea Res. I*, **52**, 241–258, doi:10.1016/j.dsr.2004.10.004.

Smith, W. H. F., and D. T. Sandwell, 1997: Global seafloor topography from satellite altimetry and ship depth soundings. *Science*, **277**, 1956–1962, doi:10.1126/science.277.5334.1956.

Winton, M., 2000: A reformulated three-layer sea ice model. *J. Atmos. Oceanic Technol.*, **17**, 525–531, doi:10.1175/1520-0426(2000)017<0525:ARTLSI>2.0.CO;2.

Wyrtki, K., 1961: The flow of water into the deep-sea basins of the western South Pacific Ocean. *Aust. J. Mar. Freshwater Res.*, **12**, 1–16, doi:10.1071/MF9610001.

Zenk, W., and E. Morozov, 2007: Decadal warming of the coldest Antarctic Bottom Water flow through the Vema Channel. *J. Geophys. Res.*, **34**, L14607, doi:10.1029/2007GL030340.